

Direct Simulation Monte Carlo: Novel Applications and New Extensions

Alejandro L. Garcia
Department of Physics, San Jose State University
San Jose, CA 95192-0106
agarcia@jupiter.sjsu.edu

and

Florence Baras
Center for Nonlinear Phenomena and Complex Systems
Université Libre de Bruxelles, Campus Plaine, C.P. 231
1050 Brussels, Belgium
fbaras@ulb.ac.be

January 9, 1997

Abstract

Direct Simulation Monte Carlo (DSMC) is a particle-based simulation method for gas dynamics. The method can be viewed as either a simplified molecular dynamics (DSMC being several orders of magnitude faster) or as a Monte Carlo method for solving the time-dependent nonlinear Boltzmann equation. The DSMC method has been used successfully in the study of rarefied gas flows for several decades but has recently found new applications in chemistry and physics. After outlining the method, novel applications (microchannel and surface dynamics studies, hydrodynamic and chemical fluctuations) and recent extensions (dense gas and liquid-vapor dynamics) of the method are described.

1 Introduction

The atomic hypothesis, and its use in explaining physical and chemical phenomena, is so pervasive today that we sometimes forget that its validity was seriously debated only 100 years ago. Ernst Mach wrote “[The] efforts of thinkers have always been bent upon the ‘reduction of all physical processes to the motion of atoms,’ . . . This ideal has often played an effective part in popular lectures, but in the workshop of the serious inquirer it has discharged scarcely the least function.” [1] Even today, the continuum description of fluids is sufficiently accurate and complete as to be used to calculate flows for hurricanes, aircraft, turbines, lungs, and candle flames. While we no longer doubt that a gas is a collection of molecules in constant motion, physical and chemical gas dynamics calculations rarely need to consider this microscopic description. The properties of a dilute gas may be obtained from kinetic theory (e.g., Chapman-Enskog transport coefficients, Arrhenius rate constants), yet once these macroscopic properties are determined, a continuum description, such as the Navier-Stokes equations, can usually be used.

In this paper we consider physical and chemical problems in which a continuum description of a gas is *not* accurate. The continuum formulation breaks down when the characteristic length scale in our system is comparable to the mean free path for molecules in the gas. From kinetic theory, the mean free path in a gas is

$$\lambda = \frac{1}{\sqrt{2}\pi\sigma^2n}, \quad (1)$$

where n is the number density and σ is the effective diameter of the molecules. For air at atmospheric pressure, the mean free path is approximately 50 nm (about the wavelength of visible light) while in the rarefied upper atmosphere (120 km altitude), the mean free path is several meters. One defines the Knudsen number as $\text{Kn} = \lambda/L$, where L is the characteristic length scale of the physical system. In general, the continuum description is no longer accurate when $\text{Kn} > 1/10$, as indicated in Figure 1. Various examples of high Knudsen number flows are illustrated in Figure 2.

The discrete nature of a gas also manifests itself in spontaneous fluctuation phenomena (e.g., the Rayleigh light scattering that makes the sky blue). In a dilute gas, the number of particles within a cubic mean free path is large (about 3000 molecules for air at STP) so fluctuation phenomena are only apparent at large Knudsen number.

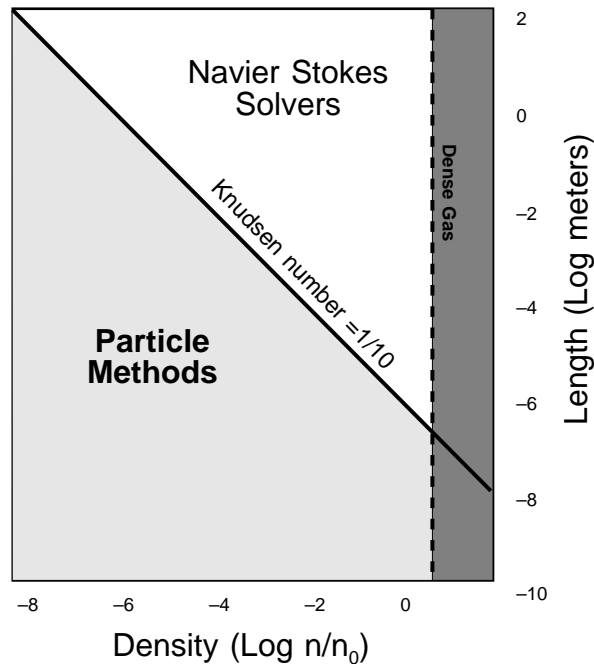


Figure 1: Regimes of a gas as functions of density (relative to air at STP) and length scale. Continuum description becomes inaccurate when the characteristic length scale is within an order of magnitude of the mean free path. Adapted from [5].

Since high Knudsen number problems arise under extreme conditions (pressures near vacuum or at nanometer length scales), laboratory experiments are difficult to perform. In recent years, this field of fluid mechanics has greatly profited by the introduction of particle-based algorithms for the simulation of gas dynamics. For physicists and chemists, the most well-known particle method is molecular dynamics (MD). [2] In MD simulations, the trajectory of every particle in the fluid is computed from Newton’s equations given an empirically determined interparticle potential. Simple hydrodynamic phenomena, such as von Kármán vortex shedding [3] and Rayleigh-Bénard convection [4], have been observed using molecular dynamics. Yet even running on the most powerful machines today MD simulations of a dilute gas are extremely time consuming. The reason is that the execution time of the simulation depends on either the computational time step relative to the mean free time (for continuous potentials) or the number of molecules within a mean free path radius (for “hard” potentials). In a liquid both of these quantities are of order one but in a gas they are of order 10^3 or greater. Fortunately, there are alternative algorithms for simulating a dilute gas.

The direct simulation Monte Carlo (DSMC) method is a particle-based, numerical scheme for solving the nonlinear Boltzmann equation. [5, 6] Rather than exactly calculating successive collisions, as in MD, the DSMC method generates collisions stochastically with scattering rates and post-collision velocity distributions determined from the kinetic theory of a dilute gas. While DSMC simulations are not

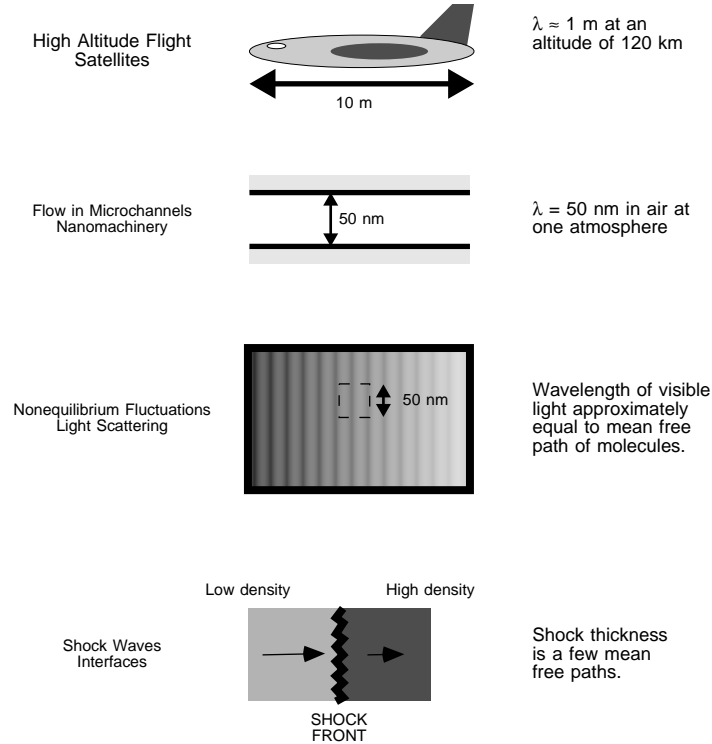


Figure 2: High Knudsen number scenarios.

correct at the length scale of an atomic diameter (e.g., pair correlation function is not recovered) they are accurate at scales smaller than a mean free path. The algorithm has been thoroughly tested in large Knudsen number flow problems over the past 20 years and found to be in excellent agreement with both experimental data [7] and molecular dynamics computations [8, 9].

Since its introduction, the DSMC method has been primarily used to compute rarefied gas flows in aeronautics. The method's scope has expanded in recent years and this paper presents a variety of recent applications of DSMC *outside* of the field of aerospace engineering. Since this article is directed to a broad audience of scientists, the next section presents a summary of the algorithm. The sections that follow present applications to nanoscale flows near surfaces, hydrodynamic and chemical fluctuations and an extension of the DSMC method to non-ideal gases (e.g., Van der Waals equation of state).

2 Direct Simulation Monte Carlo

This section presents a summary of the Direct Simulation Monte Carlo method; for more detailed expositions see [5] or [10]. In a DSMC simulation, the state of the system is given by the positions and velocities of particles, $\{\vec{r}_i, \vec{v}_i\}$. First, the particles are moved as if they did not interact, that is, their positions are updated to $\vec{r}_i + \vec{v}_i \Delta t$. Any particles that reach a boundary are processed according to the appropriate boundary condition. Second, after all particles have been moved, a given number are randomly selected for collisions. This splitting of the evolution between streaming and collisions is only accurate when the time step, Δt , is a fraction of the mean collision time for a particle.

Typically each particle in the simulation represents thousands of molecules in the physical system. In this sense, the DSMC method solves the Boltzmann equation using a representative random sample drawn from the actual velocity distribution. This rescaling allows us to model many systems of interest using only $10^4 - 10^5$ particles (though simulations using over 10^8 particles are not uncommon). However, if the number of particles in the simulation is too small, fewer than about 20 particles per cubic mean

free path, the DSMC method is not accurate. [11]

2.1 Collisions

The concept of “collision” implies that the interaction potential between particles is short-ranged. For simplicity, in this section the DSMC algorithm is formulated for a dilute gas of hard sphere particles with diameter σ and mass m . For engineering applications, more realistic representations of the molecular interaction may be used to give accurate transport properties [5] and equations of state [12] (see section 5).

To evaluate the collisions in the gas, the particles are sorted into cells whose volumes are typically a fraction of a cubic mean free path. This spatial “coarse-graining” allows two particles to collide by simply being located within the same cell; no other positional information is used in the evaluation of collisions. At each time step, particles within a cell are randomly selected as collision partners. From kinetic theory, the collision probability for hard spheres is linearly proportional to their relative velocity. If particles i and j are selected as candidates for a collision, they are accepted as collision partners if

$$|\vec{v}_i - \vec{v}_j| > \mathcal{R}v_r^{max}, \quad (2)$$

where v_r^{max} is the local maximum relative speed and \mathcal{R} is a uniform deviate in $[0, 1)$. Since only the magnitude of the relative velocity between particles is used in determining their collision probability, even particles that are moving away from each other may collide.

An interesting variant of DSMC, first suggested by Nanbu [13], has only one particle’s velocity affected at each collision (its collision partner assumed to come from a local pool of available partners). While this variant initially appeared promising, it is flawed in that it does not conserve energy (e.g., an isolated system will systematically cool). [14]

Conservation of momentum and energy provide four of the six equations needed to determine the post-collision velocities. The remaining two conditions are selected at random with the assumption that the direction of the post-collision relative velocity is uniformly distributed in the unit sphere. This assumption is exact for hard sphere particles at low densities and has been found to be an excellent approximation in general. [15]

The last step of the collision process is to determine how many collisions should occur in a cell during a time step Δt . The collision rate (per unit time per unit volume) for a dilute hard sphere gas is

$$\Lambda = \frac{1}{2}n^2\pi\sigma^2\langle v_r \rangle, \quad (3)$$

where n is the number density and $\langle v_r \rangle$ is the mean relative speed between particles. Instead of calculating Λ , which would require computing $\langle v_r \rangle$ in each cell at each time step, we use the fact that the fraction of candidate collision partners that are accepted is proportional to $\langle v_r \rangle / v_r^{max}$ (see equation (2)). The number of candidate collision partners (per unit time per unit volume), including those rejected, is taken to be $\frac{1}{2}n^2\pi\sigma^2v_r^{max}$. This procedure is correct even if we have only an estimate for v_r^{max} , so long as the true maximum relative speed is smaller than our estimate. This procedure for evaluating the collision rate is known as the NTC (No Time Counter) method; early DSMC programs used a “time counter” to assign a random time duration after each collision. [5]

2.2 Boundaries

DSMC simulations employ various types of boundaries (e.g., specular surfaces, thermal walls, fluxing reservoirs). When a particle strikes a specular surface its component of velocity normal to the surface is reversed. When a particle strikes a perfect thermal wall, at temperature T_w , all three components of velocity are reset according to the biased-Maxwellian distribution. The component normal to the wall is distributed as,

$$P_{\perp}(v_{\perp}) = \frac{m}{kT_w}v_{\perp}e^{-mv_{\perp}^2/2kT_w}, \quad (4)$$

while each parallel component is distributed as

$$P_{\parallel}(v_{\parallel}) = \sqrt{\frac{m}{2\pi kT_w}}, e^{-mv_{\parallel}^2/2kT_w} \quad (5)$$

where k is Boltzmann's constant. Note that the former distribution is biased because the faster particles strike the wall more frequently and, by reciprocity, the distribution for particles leaving the thermal wall must reflect this bias. A surface may not fully thermalize all scattered molecules. In the simple Maxwell model of accommodation, with probability α the particle's velocity is thermalized by the wall and with probability $(1 - \alpha)$ the particle is specularly reflected by the wall.

In reality, gas-surface scattering is more complex. Molecular beam experiments can measure the distribution function $P(\vec{v}'|\vec{v})$, where \vec{v} is the velocity of a particle arriving at a surface and \vec{v}' is its velocity leaving the surface [16]. This distribution function can be directly implemented in the subroutine that handles boundary reflections in a DSMC program. Statistical mechanics demands that the scattering distribution must satisfy the reciprocity (or detailed balance) condition, [17]

$$v'_\perp P(-\vec{v}'|\vec{v})e^{-mv'^2/2kT_w} = -v_\perp P(\vec{v}'|\vec{v})e^{-mv^2/2kT_w}. \quad (6)$$

Some experimentally reported scattering distributions are curve-fits that do not satisfy the reciprocity condition. Such distributions cannot be used directly in a DSMC simulation because spurious results will occur (e.g., gas will spontaneously start convective motion at thermodynamic equilibrium).

A realistic distribution that satisfies reciprocity is given by Cercignani and Lampis. [18] The distributions of the parallel and perpendicular components are assumed to be uncorrelated and given by

$$P_\parallel(\tilde{v}'_\parallel|\tilde{v}_\parallel) = \frac{1}{\sqrt{\pi\sigma_\parallel(2-\sigma_\parallel)}} \exp\left(-\frac{[\tilde{v}'_\parallel - (1-\sigma_\parallel)\tilde{v}_\parallel]^2}{\sigma_\parallel(2-\sigma_\parallel)}\right), \quad (7)$$

where σ_\parallel is the accommodation coefficient for momentum parallel to the surface and

$$P_\perp(\tilde{v}'_\perp|\tilde{v}_\perp) = \frac{2v'_\perp}{\alpha_\perp} I_0\left(\frac{2}{\alpha_\perp}\sqrt{1-\alpha_\perp}\tilde{v}'_\perp\tilde{v}_\perp\right) \times \exp\left(-\frac{\tilde{v}_\perp^2 + (1-\alpha_\perp)\tilde{v}'_\perp^2}{\alpha_\perp}\right), \quad (8)$$

where I_0 is the modified Bessel function of the first kind and α_\perp is the accommodation coefficient for kinetic energy normal to the surface ($\frac{1}{2}mv_\perp^2$). The velocities in the distributions are normalized such that $v = \tilde{v}\sqrt{2kT_w/m}$. A simple method for sampling from these distributions is given by Lord.[19]

Finally, boundaries can act as fluxing reservoirs, that is, as infinite, equilibrium thermal baths at fixed temperature and density. At each time step, particles from the reservoirs flux into the system while particles already in the system can flux out. A flow velocity may be assigned to a reservoir to model inflow or outflow boundaries.

2.3 Statistics

Since DSMC is inherently a stochastic method, most physical quantities of interest are computed as time averages. The values of mass density, $\hat{\rho}(\vec{r}, t)$, momentum density, $\hat{\vec{p}}(\vec{r}, t)$ and energy density $\hat{e}(\vec{r}, t)$ are periodically measured as

$$\left\{ \begin{array}{l} \hat{\rho}(\vec{r}, t) \\ \hat{\vec{p}}(\vec{r}, t) \\ \hat{e}(\vec{r}, t) \end{array} \right\} = \frac{1}{V_c} \sum_i^{\text{Cell at } \vec{r}} \left\{ \begin{array}{l} m \\ m\vec{v}_i \\ \frac{1}{2}m|\vec{v}_i|^2 \end{array} \right\}, \quad (9)$$

where the caret indicates these are instantaneous, fluctuating values and the sum is over particles in the statistics cell (of volume V_c) located at \vec{r} . For steady flows, the fluid velocity is computed as $\vec{u}(\vec{r}) = \hat{\vec{p}}(\vec{r})/\hat{\rho}(\vec{r})$ using the time averaged values of mass and momentum density. Temperature is computed from the equipartition theorem as

$$T(\vec{r}) = \frac{2m}{3k} \left[\frac{e(\vec{r})}{\rho(\vec{r})} - \frac{1}{2}|\vec{u}(\vec{r})|^2 \right]. \quad (10)$$

The local pressure $P(\vec{r})$ may be evaluated from the ideal gas law or by explicitly evaluating the pressure tensor. [20] The two results may not be equivalent since under some conditions (e.g., high Mach number) the pressure tensor will not be isotropic. The force on a wall may be directly computed from the time averaged change in the momentum of particles striking the wall. [10]

3 Flows in Nanochannels

Micro-electrical-mechanical systems (MEMS) are micron-size devices fabricated using photolithographic techniques. Examples of MEMS include micro-sensors, micro-valves and micro-motors. Since many MEMS have a gas flow as an integral part of the device, there has recently been much interest in high Knudsen number flows in nanometer-scale channels. [21]

Another example of a nanochannel exists in a computer disk drive. The drive's read/write head floats less than fifty nanometers above the surface of the spinning platter so the Knudsen number for this flow is order unity. [22]. The head is supported above the platter by the lubrication effect, as observed when a sheet of paper glides easily when thrown across a smooth table. The prediction of the vertical force on the head (as obtained from the pressure distribution in the gas) is a crucial design calculation. The head will not accurately read or write if it flies too high since the sensitivity decreases exponentially with distance from the platter. If the head flies too low, it can accidentally scratch the surface of the disk or even catastrophically "crash" into the platter.

The head and platter together with the gas layer in between form a slider air bearing. Consider a channel formed by a stationary, slightly inclined surface above a horizontal surface, as illustrated in Figure 3. The lower surface moves with velocity U in the x direction. A dilute gas occupies the space between the surfaces. The gas and the surfaces are assumed to be at a constant, ambient temperature, T_0 . Since the incline is slight, typically less than one degree, the pressure in the gas, p , is taken to be constant in the vertical direction. At the left ($x = 0$) and right ($x = L$) boundaries, the pressure in the gas is fixed at ambient pressure, p_0 .

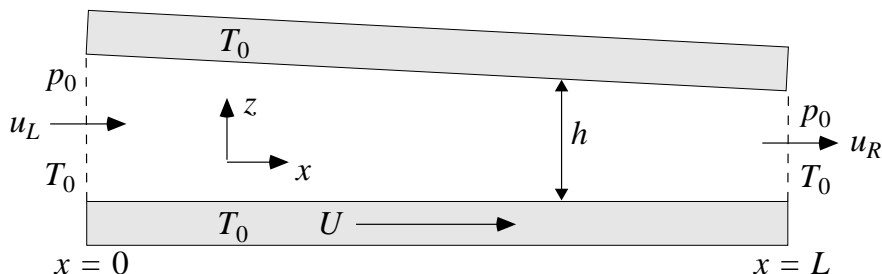


Figure 3: Geometry of a simple wedge slider bearing.

From standard lubrication theory [23], the pressure in the gas may be computed from the Reynolds equation,

$$\frac{d}{dX} \left(PH^3 \frac{dP}{dX} \right) = \Lambda_B \frac{d}{dX} (PH), \quad (11)$$

where $X = x/L$, $P = p/p_0$, $H = h/h_0$, and $h(x)$ is the vertical spacing between the walls; the minimum spacing is $h_0 = h(x = L)$. The bearing number is $\Lambda_B \equiv 6\eta UL/p_0 h_0^2$ where η is the dynamic viscosity of the gas.

It was first pointed out by Maxwell that the velocity of a gas near a moving wall does not match the wall's velocity; this phenomenon is known as "velocity slip." [24] Specifically, the difference between the velocity of the wall and the velocity of the gas near the wall is $\ell \nabla_{\perp} \vec{u}$ where $\nabla_{\perp} \vec{u}$ is the velocity gradient normal to the wall. The slip length, ℓ , is often approximated as being equal to the mean free path. However, this simple formulation for velocity slip is not accurate at large Knudsen number. [8]

A slip correction was first introduced into the Reynolds equation by Burgdorfer [25] as

$$\frac{d}{dX} \left([1 + 6\text{Kn}] PH^3 \frac{dP}{dX} \right) = \Lambda_B \frac{d}{dX} (PH), \quad (12)$$

where $\text{Kn} = \lambda/h$ is the local Knudsen number. Fukui and Kaneko [26] developed a more sophisticated formulation,

$$\frac{d}{dX} \left(\bar{Q}_p(\text{Kn}) PH^3 \frac{dP}{dX} \right) = \Lambda_B \frac{d}{dX} (PH). \quad (13)$$

The function $\overline{Q}_p(\text{Kn})$ is the non-dimensional flow rate for Poiseuille flow; a database of tabulated values for $\overline{Q}_p(\text{Kn})$ is given in [27].

Figure 4 shows data (open and filled symbols) from DSMC simulations (16000 particles), dotted line is equation (11), dash line is equation (12) and solid and dash-dot lines are equation (13) with accommodation coefficients of 1.0 and 0.9, respectively. Parameters are $h_0 = 25$ nm, $h(x=0) = 2h_0$, $p_0 = 1$ atm, $T_0 = 273$ K, $U = 25$ m/s, and $L = 5\mu\text{m}$. The simulation uses a Cercignani-Lampis surface scattering model with the accommodation properties obtained from molecular beam experiments performed on actual disk drive platters. [28] The sides are reservoirs at ambient density and temperature with flow velocity adjusted so as to maintain ambient pressure at these inflow and outflow boundaries. Note the close agreement between the DSMC simulation data and the Fukui-Kaneko theory. Other results for different configurations are given in [29]; similar DSMC results have been obtained by others [30, 31].

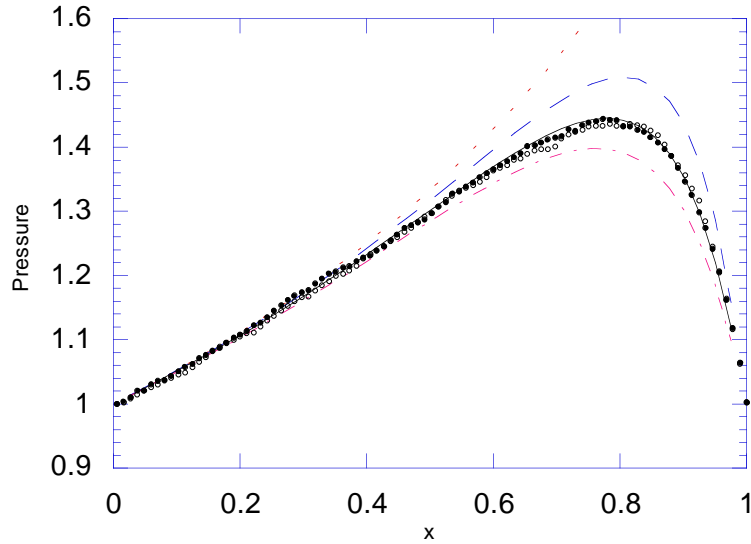


Figure 4: Pressure distribution for a slider bearing.

4 Hydrodynamic and Chemical Fluctuations

4.1 Hydrodynamic fluctuations

Fluctuating hydrodynamics is a stochastic formulation of the Navier-Stokes equations. [32] Spontaneous fluctuations of hydrodynamic variables are introduced by the addition of random components to the shear stress and heat flux. Since these fluxes are not conserved quantities, they are short-lived and short-ranged such that, at hydrodynamic scales, their random components are assumed to be Dirac-delta correlated in time and space. The magnitudes of these random fluxes are set by the condition that at thermodynamic equilibrium one recovers the Gibbs distribution. [33]

Consider a one-dimensional system consisting of a dilute gas between thermal walls located at $y = 0$ and $y = L$; the walls are stationary but at different temperatures. The stochastic hydrodynamic equations for the fluctuations of density ($\delta\rho$), y -velocity (δv) and temperature (δT) are,

$$\frac{\partial}{\partial t}\delta\rho = -\frac{\partial}{\partial y}\rho_0\delta v \quad (14)$$

$$\rho_0\frac{\partial}{\partial t}\delta v = -R\frac{\partial}{\partial y}(T_0\delta\rho + \rho_0\delta T) + \frac{4}{3}\frac{\partial}{\partial y}\eta_0\frac{\partial}{\partial y}\delta v - \frac{\partial}{\partial y}\sigma_{yy} \quad (15)$$

$$\frac{3}{2}\rho_0 R\frac{\partial}{\partial t}\delta T = -\frac{3}{2}\rho_0 R\delta v\frac{\partial}{\partial y}T_0 - R\rho_0 T_0\frac{\partial}{\partial y}\delta v$$

$$+\frac{\partial^2}{\partial y^2}\kappa_0\delta T - \frac{\partial}{\partial y}g_y, \quad (16)$$

where η and κ are the shear viscosity and thermal conductivity, $R = k/m$ is the gas constant, and the subscript 0 indicates mean values. The fluctuating shear stress and heat flux have zero mean and variances,

$$\langle\sigma_{yy}(y,t)\sigma_{yy}(y',t')\rangle = \frac{8k\eta T_0}{3S}\delta(y-y')\delta(t-t') \quad (17)$$

$$\langle g_y(y,t)g_y(y',t')\rangle = \frac{2k\kappa T_0^2}{S}\delta(y-y')\delta(t-t'), \quad (18)$$

where S is the crosssectional area of the system.

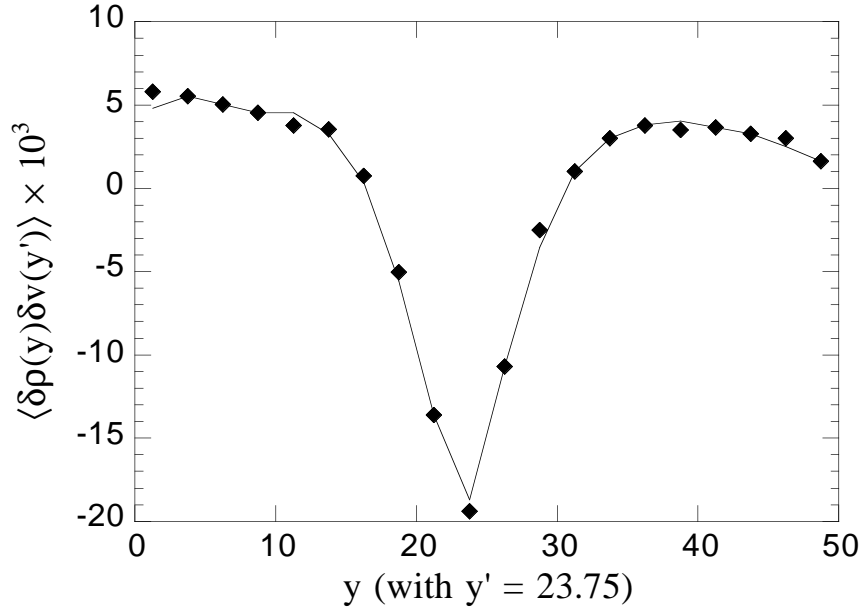


Figure 5: Correlation of density-velocity fluctuations in a dilute gas under a temperature gradient.

In equilibrium these equations may be used to compute the correlation of fluctuations from which one obtains the Rayleigh-Brillouin light scattering spectrum. [34] The equal-time spatial correlations of fluctuations are delta-correlated at equilibrium. Out of equilibrium (e.g., in a temperature gradient) the correlation functions are modified and the effects may (with great difficulty) be observed in light scattering experiments. [35]

These nonequilibrium fluctuations are easily observed in DSMC simulations. Figure 5 shows the equal-time spatial correlation density and velocity fluctuations for a system with a temperature gradient. [36] Data points are from a DSMC simulation (20000 particles, $L = 50\lambda$, 5×10^9 collisions); solid line is a numerical solution of the fluctuating hydrodynamic equations. Temperature ratio of the walls is 3:1. Note the long range nature of the correlation; this nonequilibrium correlation creates an asymmetry in the Brillouin spectrum lines. Also note the good agreement between DSMC simulation and the numerical solution of the fluctuating hydrodynamic equations. Figure 6 shows the nonequilibrium velocity correlation for a system under a constant shear (the equilibrium delta-function contribution to the correlation function has been removed). [37] Data points are from a DSMC simulation (20000 particles, $L = 50\lambda$, 10^9 collisions); solid line is a numerical solution of the fluctuating hydrodynamic equations. Wall speed is about twice the sound speed. Similar results were recently obtained in molecular dynamics simulations. [38] We plan to extend this study to fluctuations near hydrodynamic instabilities. [39]

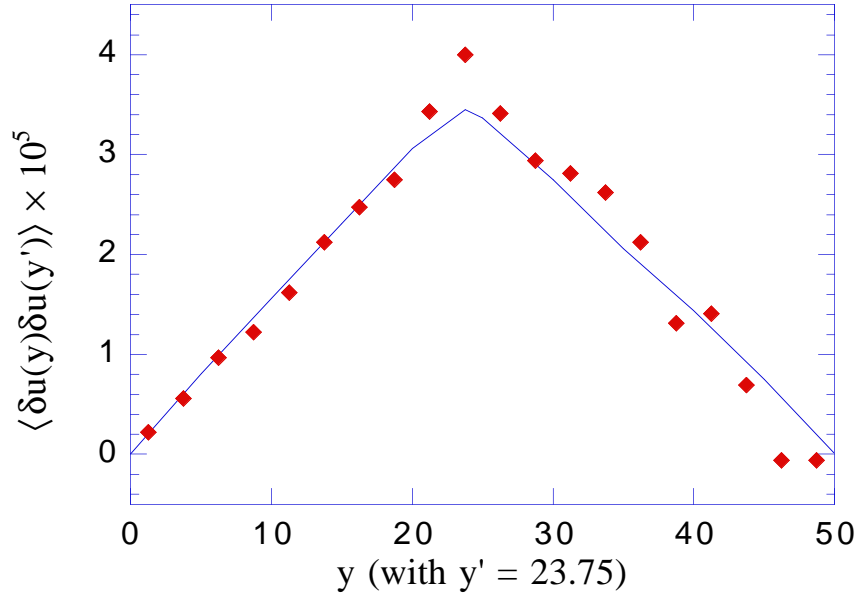


Figure 6: Correlation of velocity fluctuations in a dilute gas under a constant shear.

4.2 Chemical fluctuations

We now consider fluctuations in a dilute gas with chemical reactions. In simplified hard sphere chemistry, all molecules are identical except for a label (or “color”) identifying their species. [40] A random fraction of collisions is taken to be reactive; in these collisions the colors of the particles are changed according to the appropriate chemical step that occurred.

First consider a homogeneous system (e.g., continuously stirred tank reactor) in which the chemical system has a bifurcation of its steady state. Since the DSMC method allows for only binary collisions, we consider the chemical reaction scheme: [41]



where the concentration of S (solvent) particles is held fixed. The macroscopic rate equations corresponding to the above scheme are,

$$\begin{aligned}
 \frac{du}{dt} &= -k_1 u w + \alpha(u_f - u) \\
 \frac{dv}{dt} &= k_1 u w - 2(k_2 v^2 - k_{-2} w s) - k_3 v s + \alpha(v_f - v) \\
 \frac{dw}{dt} &= k_2 v^2 - k_{-2} w s,
 \end{aligned} \tag{20}$$

where u , v , w , and s are the mole fractions of U , V , W , and S , respectively. The reactions take place in a feed tank with α being the inverse residence time (feed rate); u_f and v_f are the feed mole fractions of U and V , respectively. The system is assumed to be impermeable to W .

In the DSMC simulations, the feed process may be implemented via two supplementary reactions:



In each case the forward reaction mimics the inflow and the reverse reaction the outflow of U or V . The rates are $a_+ = 2\alpha u_f/s^2$, $b_+ = 2\alpha v_f/s^2$, and $a_- = b_- = \alpha/s$. To maintain the concentration of species S fixed, we introduce an inert species A . Anytime there is a deficit (or surplus) of solvent molecules, an inert molecule is converted into an S (or vice versa). [42]

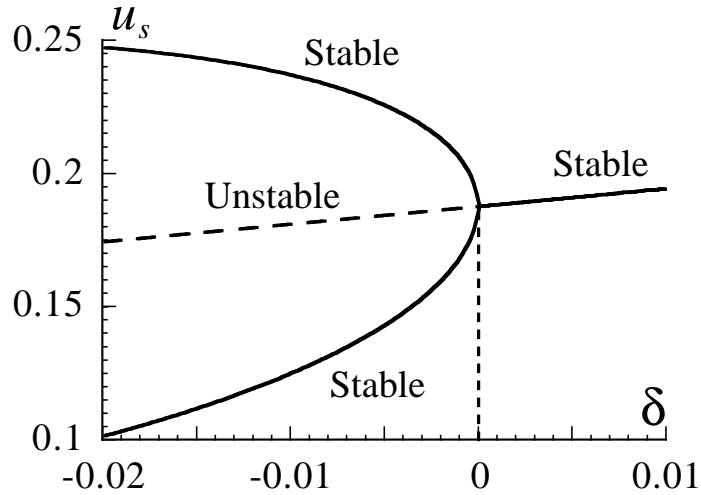


Figure 7: Stability diagram for u as a function of $\delta = v_f - u_f/8$.

For certain parameter values, the macroscopic equations, (20), can admit multiple steady states or limit cycle oscillations. [43] For example, a pitchfork bifurcation in u is illustrated in Figure 7; parameters are: $k_1 = 1$, $k_2 = \frac{1}{2}$, $k_{-2} = \frac{1}{26s}$, $\alpha = 0.28$, $u_f = \frac{1}{4}$, and $k_3 = \frac{u_f + v_f}{3s} \sqrt{2\alpha \frac{k_1 k_2}{s k_{-2}} \frac{u_f + v_f}{u_f - 2v_f} - \frac{\alpha}{s}}$. Because the bifurcation is asymmetrical, past the bifurcation point we expect one branch to be more probable than the other. From the associated Langevin equations for this model, one finds that the upper branch should be preferred. However, the Master equation formulation predicts that the lower branch has higher probability. The probability distribution of u shown in Figure 8 was measured in a DSMC simulation (circles) with 2000 particles run for 2×10^9 total collisions; the numerical solutions of the Langevin equation (dashed curve) [44] and the Master equation (solid curve) [45] are also shown. Clearly the DSMC simulation is in excellent agreement with the Master equation calculation.

Next we examine fluctuations in a spatially extended chemical system. Consider the simple reaction scheme: [46]



where the solvent (S) concentration is held fixed. Again, the particle simulation introduces an inert species A to impose this constraint. We consider a one-dimensional system with periodic boundary conditions and which, for the purposes of statistical measurement only, is partitioned into N_c cells. The spatial nonequilibrium correlation for species U is,

$$g_{i,j} \equiv \langle (U_i - \langle U \rangle)(U_j - \langle U \rangle) \rangle - \langle U \rangle \delta_{ij}, \quad (23)$$

where U_i is the number of U molecules in cell i . At thermodynamic equilibrium $g_{i,j} = 0$ since equal-time density fluctuations are uncorrelated in space. With the concentration of S held fixed, the system is maintained at a nonequilibrium steady state and Figure 9 shows $g_{i,j}$ in this state. The solid curve is from a numerical solution of the Master equation; data points are from a DSMC simulation (42000 particles run for over 10^{10} total collisions). System length is $L = 3780\sigma$, $n/\sigma^3 = 5 \times 10^{-3}$, $k_1 = 0.1$, $k_2 = 0.15$,

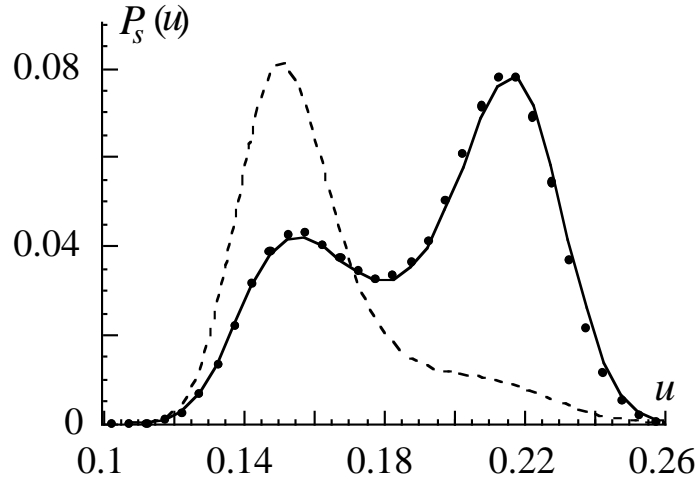


Figure 8: Probability distribution of u for $\delta = -0.003$

$k_3 = 0.4$, and $s = 0.1$. Note the good agreement between DSMC simulation and the numerical solution of the Master equation.

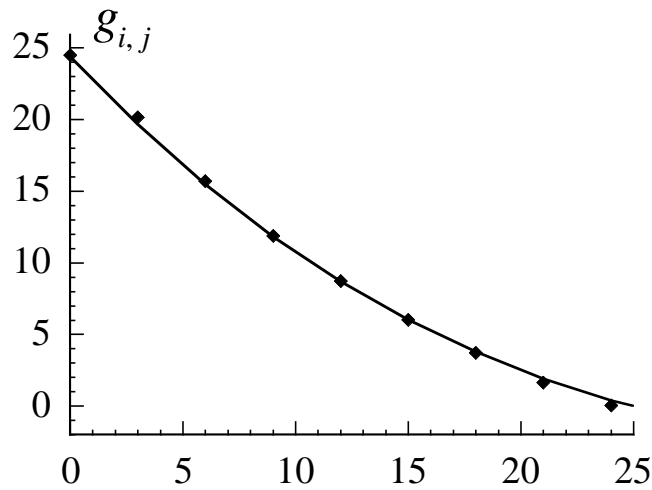


Figure 9: Spatial correlation function $g_{i,j}$ versus $|i - j|$ for (22).

Finally, consider the previous reaction scheme, (19), in a one dimensional system for the parameters that yield a bifurcation in the steady state solutions. Far from the bifurcation point the dynamics can be linearized about the reference state and the resulting correlations are similar to the previous result. On approaching the bifurcation point, a significant lengthening of the decay time of fluctuations is observed. This “critical slowing down” in turn induces long range spatial correlation. Figure 10 illustrates this behavior for $\delta = 10^{-2}$ (dashed line) and 3×10^{-3} (solid line). Curves are from a numerical solution of the Master equation; data points are from a DSMC simulation (42000 particles run for over 10^{11} total collisions). System length is 3780σ and $n/\sigma^3 = 5 \times 10^{-3}$; other parameters are as in Fig. 7. Again notice the good agreement between DSMC simulation and numerical solutions of the Master equation.

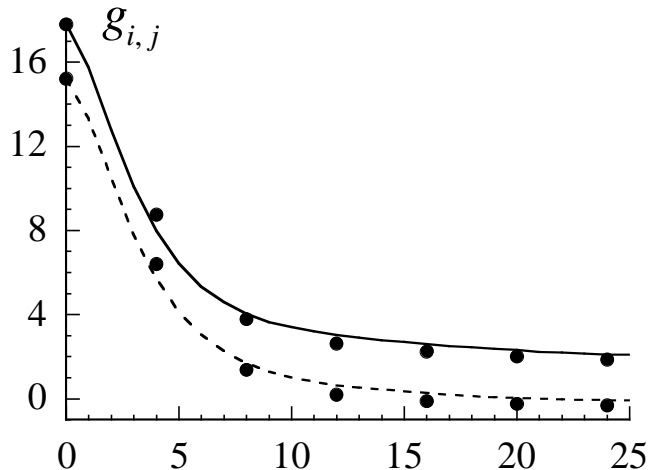


Figure 10: Spatial correlation function $g_{i,j}$ versus $|i-j|$ for (19).

5 Non-ideal Gas DSMC

The Boltzmann equation and its Chapman-Enskog expansion yield the transport properties for a dilute gas of hard spheres (HS) of diameter σ , yet have an *ideal gas* equation of state. The standard DSMC algorithm, being a Monte Carlo method for solving the Boltzmann equation, also contains this inconsistency. Modified collision rates are commonly used in DSMC to reproduce the transport properties of non-hard sphere gases (e.g., the Maxwell molecule and Bird's variable hard sphere model [5]), however these modifications retain the ideal gas equation of state (see also [47]). Naturally, at low densities the virial corrections to the equation of state are small, making the results useful despite the inconsistency.

To obtain a consistent equation of state, DSMC must be modified in the collision step to include the extra separation that particles experience if they collide as hard spheres. Consider, for example, a one dimensional system consisting of two hard sphere particles initially traveling toward each other. At the moment of collision, their separation is clearly one diameter. After the collision, the distance between the centers of the spheres will be larger than the separation between similar point particles by a distance 2σ . In three dimensions this effect generalizes to a displacement, \vec{d} :

$$\vec{d} = \frac{(\vec{v}'_1 - \vec{v}'_2) - (\vec{v}_1 - \vec{v}_2)}{|(\vec{v}'_1 - \vec{v}'_2) - (\vec{v}_1 - \vec{v}_2)|} \sigma = \frac{\vec{v}'_r - \vec{v}_r}{|\vec{v}'_r - \vec{v}_r|} \sigma, \quad (24)$$

where the incoming velocities of the colliding particles 1 and 2 are \vec{v}_1 and \vec{v}_2 , and the post-collisional velocities are \vec{v}'_1 and \vec{v}'_2 respectively. Thus, particle 1 is displaced by the vector distance \vec{d} and particle 2 by $-\vec{d}$ (see Figure 11 for an illustration of this process). Note that the vector $\vec{v}'_r - \vec{v}_r$ points in the direction of the apse line (line passing through the centers of the molecules at the moment of closest approach). [20]

The pressure in a hard sphere gas may be defined as [48]

$$P = nkT + \frac{1}{3} \frac{m}{tV} \sum_{\text{collisions}} \Delta \vec{v}_{ij} \cdot \vec{r}_{ij}, \quad (25)$$

where $\Delta \vec{v}_{ij} \cdot \vec{r}_{ij}$ is the virial (the projection of the velocity change onto the line connecting centers of colliding particles) and the sum is over all collision occurring during a time t . This may be rewritten in terms of the collision rate as,

$$P = nkT + \frac{1}{3} m \Lambda \Theta, \quad (26)$$

where $\Theta \equiv \langle \Delta \vec{v}_{ij} \cdot \vec{r}_{ij} \rangle$ is the virial averaged over collisions and Λ is the collision rate (per unit time per unit volume). Using the displacement (24) gives an average virial of $\Theta = \sigma \sqrt{\pi kT/m}$ so with the

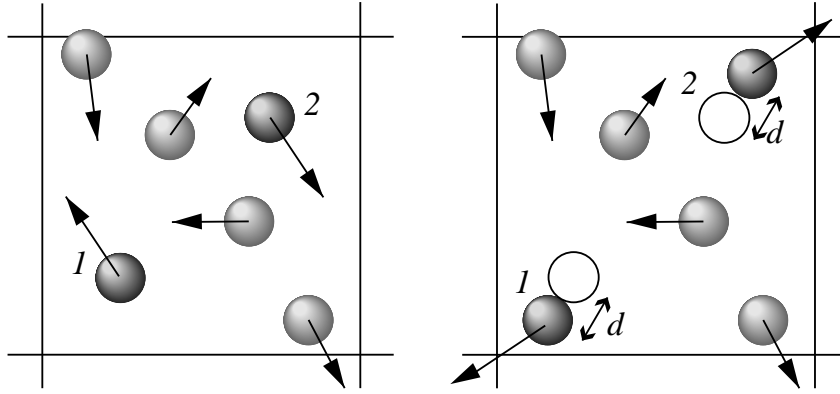


Figure 11: Schematic illustration of the displacement occurring after a collision.

Boltzmann collision rate (3) we have $P = nkT(1 + b_2n)$ where $b_2 = (2/3)\pi\sigma^3$ is the HS second virial coefficient.

In addition to the displacement, we introduce the Enskog Y -factor, the enhanced probability of a collision due to the volume occupied by the spheres. [49]. This density dependent Y factor, as determined by Monte Carlo and MD simulations and expressed in the Padé form, is, [50]

$$Y(n) = \frac{1 + 0.05556782b_2n + 0.01394451b_2^2n^2 - 0.0013396b_2^3n^3}{1 - 0.56943218b_2n + 0.08289011b_2^2n^2}. \quad (27)$$

Collisions within a cell are generated with the Enskog rate $\Lambda_E = Y\Lambda$. In the Enskog approximation, the mean free path for a dense gas is $\lambda_E = 1/(\sqrt{2}\pi nY\sigma^2)$. [49]

Finally, if the magnitude of the displacement is not constant but rather is made a function of density and temperature, a general equation of state, $P(n, T)$, may be obtained. Specifically,

$$d = \frac{\sigma}{b_2nY} \left(\frac{P}{nkT} - 1 \right), \quad (28)$$

see [51] for details. The DSMC method using a displacement \vec{d} and a collision Y -factor is called the Consistent Boltzmann Algorithm (CBA).

Kinetic theory calculations and a series of computer simulations were carried out to obtain quantitative results from this model. Pressure measured as the normal momentum transfer across a plane confirms that the simulation reproduces the correct equation of state. Figure 12 shows data points from CBA simulations; lines are theoretical equations of state (EOS). Circles are ideal gas EOS ($T = 0.19$), squares are hard sphere EOS ($T = 0.19$); triangles are Van der Waals EOS ($T = 0.19$), solid diamonds are Van der Waals EOS ($T = 0.16$), and open diamonds are Van der Waals EOS ($T = 0.16$) using the Maxwell tie-line. [33] Critical temperature for this Van der Waals EOS is $T_c = 0.18$. The transport coefficients, measured numerically as well as determined analytically from their kinetic theory expressions are in good agreement with MD data and Enskog theory up to moderate densities. [12] Figure 13 shows density (solid curves) and temperature (dashed curves) versus normalized position for a Mach 2 shock wave. Total shock tube length is 70λ , upwind number density is $n/\sigma^3 = 0.1$. From Hugoniot conditions, downwind density is $n/\sigma^3 = 0.187$ for HS EOS and $n/\sigma^3 = 0.229$ for ideal gas EOS. Filled symbols mark CBA curves; open symbols mark DSMC curves.

6 Conclusions

Direct Simulation Monte Carlo has been a popular method for the calculation of high Knudsen number gas flows where conventional Navier-Stokes (NS) solvers are inaccurate. The CBA extension (see the previous section) augments its applicability to a variety of new problems involving moderately dense gases. Despite the many advantages in using DSMC, particle methods remain costly since the sampling

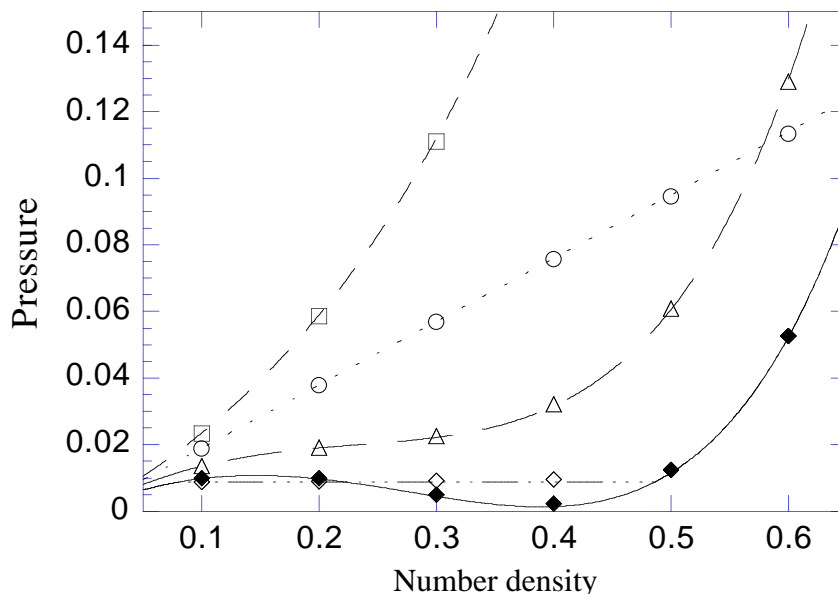


Figure 12: Pressure versus density measured in CBA simulations.

error goes as $O(\sqrt{1/N})$ where N is the number of computed time steps. In contrast, for most continuum fluid dynamics schemes, the truncation error is $O(\Delta t^2)$ so the error in the solution goes as $O(1/N^2)$.

In the future, the DSMC method will be even more powerful when used in particle-continuum hybrid codes. These hybrids will use NS solvers for the low Knudsen number parts of the flow and DSMC for the high Knudsen number regions. [52] For example, in a complex shock simulation, only the region where the shock is located would be computed using DSMC with rest of the flow handled by a NS solver. In a NS solver, for a grid size of a mean free path, the Courant-Friedrichs-Lewy stability condition requires that the time step be less than the mean free time so at microscopic scales, the time step used by the two methods is about the same. We are currently implementing a hybrid DSMC/NS program that uses Adaptive Mesh Refinement [53] to allow the simulation to span from the submicron to the centimeter scale.

Acknowledgments

The authors wish to acknowledge helpful discussions with F. Abraham, B. Alder, F. Alexander, D. Baganoff, J. Bell, D. Bogy, E. Gordon, W-D. Huang, M. Malek-Mansour, G. Nicolis, T. Olson, C. Rettner, J. W. Turner, and T. Wenski. This work was supported, in part, by the National Science Foundation's Fluid, Particulate and Hydraulic Systems Program and by the Belgian Federal Office for Technical and Cultural Affairs.

References

- [1] E. Mach, *On the Principle of the Conservation of Energy* (1894).
- [2] B. J. Alder and T.E. Wainwright, *J. Chem. Phys.* **27** 1208 (1957); M.P. Allen and D.J. Tildesley, *Computer Simulation of Liquids*, Clarendon, Oxford (1987); D.C. Rapaport, *The Art of Molecular Dynamics Simulation*, Cambridge Univ. Press, Cambridge (1995).
- [3] L. Hannon, G. Lie and E. Clementi, *J. Sc. Comp.* **1** 145 (1986); E. Meiburg, *Phys.Fluids* **29** 3107 (1986) D. C. Rapaport and E.Clementi, *Phys. Rev. Lett.* **57** 695 (1987).

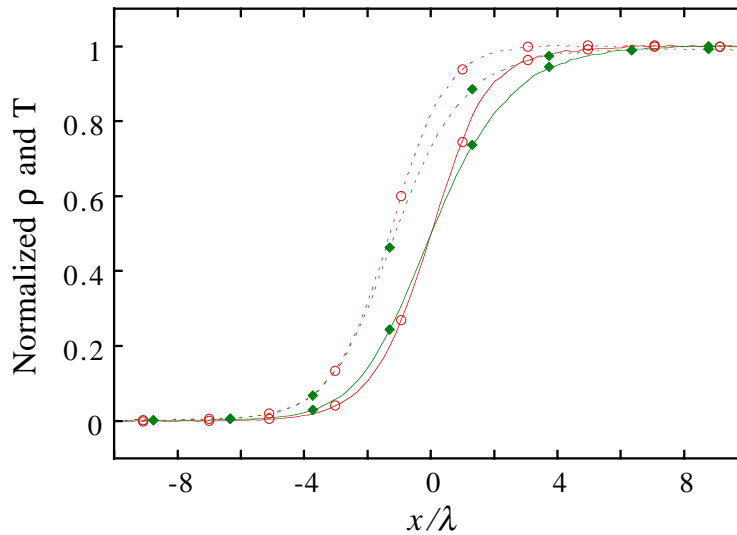


Figure 13: Density and temperature profiles in a shock wave.

-
- [4] M. Mareschal and E. Kestemont, *Nature*, **329** 427 (1987); M. Mareschal and E. Kestemont, *J. Stat. Phys.* **48** 1187 (1987); D. C. Rapaport, *Phys. Rev. Lett.* **60** 2480 (1988); M. Mareschal, M. Malek Mansour, A. Puhl and E. Kestemont, *Phys. Rev. Lett.* **61** 2550 (1988).
 - [5] G. A. Bird, *Molecular Gas Dynamics* (Clarendon, Oxford, 1976); G. A. Bird, *Molecular Gas Dynamics and the Direct Simulation of Gas Flows*, (Clarendon, Oxford, 1994).
 - [6] W. Wagner, *J. Stat. Phys.* **66**, 1011 (1992).
 - [7] E. P. Muntz, *Ann. Rev. Fluid Mech.* **21** 387 (1989); D. A. Erwin, G. C. Pham-Van-Diep and E. P. Muntz, *Phys. Fluids A* **3** 697 (1991); D. C. Wadsworth, *Phys. Fluids A* **5** 1831 (1993).
 - [8] D. L. Morris, L. Hannon and A. L. Garcia, *Phys. Rev. A* **46** 5279 (1992).
 - [9] E. Salomons and M. Mareschal, *Phys. Rev. Lett.* **69** 269 (1992).
 - [10] A. L. Garcia, *Numerical Methods for Physics*, (Prentice Hall, Englewood Cliffs, 1994).
 - [11] M. A. Fallavollita, J. D. McDonald and D. Baganoff, *Comp. Sci. Eng.* **3** 283 (1992).
 - [12] F. Alexander, A. L. Garcia, and B. Alder, *Phys. Rev. Lett.* **74** 5212 (1995); F. Alexander, A. L. Garcia, and B. Alder, in *25 Years of Non-Equilibrium Statistical Mechanics*, Eds. J. J. Brey, J. Marco, J. M. Rubi, and M. San Miguel, (Springer, Berlin, 1995).
 - [13] K. Nanbu, *J. Phys. Soc. Japan* **49** 2042 (1980).
 - [14] C. Greengard and L. Reyna, *Phys. Fluids A* **4** 849 (1992).
 - [15] G. A. Bird, in *Microscopic Simulations of Complex Hydrodynamic Phenomena*, M. Mareschal and B. L. Holian, Eds., NATO ASI Series, Vol. 292 (Plenum, New York, 1992).
 - [16] F. O. Goodman, *Prog. Surface Sci.* **5** 261 (1975).
 - [17] C. Cercignani, *Trans. Th. Stat. Phys.* **2** 27 (1972).
 - [18] C. Cercignani and M. Lampis, *Trans. Th. Stat. Phys.* **1** 101 (1971).
 - [19] R. G. Lord, *J. Fluid Mech.* **239** 449 (1992).

- [20] S. Chapman and T.G. Cowling, *The Mathematical Theory of Non-Uniform Gases*, (Cambridge Univ. Press, Cambridge, 1970).
- [21] E. B. Arkilic, M. A. Schmidt and K. S. Breuer, in *Application of Microfabrication to Fluid Mechanics*, ASME Winter Annual meeting, pg. 57 (1994); J.C. Harley, Y. Huang, H. H. Bau, and J.N. Zemel, *J. Fluid Mech.* **284** 257 (1995); E. S. Piekos and K. S. Breuer, *AIAA paper* 95-2089 (1995); C. K. Ho, E. S. Oran and B. Z. Cybyk, *AIAA paper* 95-2090 (1995); S. Fukui and R. Kaneko, in *Handbook of Micro/Nanotribology*, ed. B. Bhushan, (CRC Press, Boca Raton, 1995).
- [22] K. L. Deckert, *IBM. J. Res. Develop.* **35** 660 (1990); N. Tagawa, *Wear* **168** 43 (1993).
- [23] W. A. Gross, L. A. Matsch, V. Castelli, A. Eshel, J. H. Vohr and M. Wildmann, *Fluid Film Lubrication*, (Wiley, New York, 1980); A. Cameron and C. McEttles, *Basic Lubrication Theory*, (Ellis Horwood, Chichester, 1981).
- [24] J.C. Maxwell, *Philos. Trans. London* **170** 231 (1867); W.G. Vincenti and C.H. Kruger, *Introduction to Physical Gas Dynamics* (Krieger, Malabar, 1965).
- [25] A. Burgdorfer, *Trans. ASME* **81** 94 (1959).
- [26] S. Fukui and R. Kaneko, *J. Tribology* **110** 253 (1988).
- [27] S. Fukui and R. Kaneko, *J. Tribology* **112** 78 (1990).
- [28] C. Rettner, personal communication.
- [29] F. J. Alexander, A. L. Garcia and B. J. Alder, *Phys. Fluids* **6** 3854 (1994).
- [30] W.D. Huang and D. Bogy, personal communication.
- [31] S. Fukui and R. Kaneko, personal communication.
- [32] L. D. Landau and E. M. Lifshitz, *Fluid Mechanics* (Pergamon Press, Oxford, 1959).
- [33] L. D. Landau and E. M. Lifshitz, *Statistical Mechanics* (Pergamon Press, Oxford, 1980).
- [34] B. J. Berne and R. Pecora, *Dynamic Light Scattering*, (Krieger, Malabar, 1976); J. P. Boon and S. Yip, *Molecular Hydrodynamics*, (Dover, New York, 1980).
- [35] D. Beysens, Y. Garrabos, and G. Zalczer *Phys. Rev. Lett.* **45** 403 (1980); G. H. Wegdam, N. M. Keulen, and J. C. F. Michielsen, *Phys. Rev. Lett.* **55** 630 (1985).
- [36] M. Malek Mansour, A. L. Garcia, G. C. Lie and E. Clementi, *Phys. Rev. Lett.* **58**, 874 (1987).
- [37] A. L. Garcia, M. Malek Mansour, G. Lie, M. Mareschal, and E. Clementi, *Phys. Rev. A* **36** 4348 (1987).
- [38] M. Mareschal, M. Malek Mansour, G. Sonnino, and E. Kestemont, *Phys. Rev. A* **45** 7180 (1992).
- [39] A. L. Garcia and C. Penland, *J. Stat. Phys.* **64** 1121 (1991).
- [40] J. Portnow, *Phys. Lett. A* **51** 370 (1975); P. Ortoleva and S. Yip, *J. Chem. Phys.* **65** 2045 (1976).
- [41] F. Baras, J.E. Pearson and M. Malek Mansour, *J. Chem. Phys.* **93** 5747 (1990).
- [42] J. Boissonade, *Phys. Lett. A* **74** 285 (1979).
- [43] G. Nicolis *Introduction to Nonlinear Science* (Cambridge Univ. Press, Cambridge, 1995).
- [44] A. L. Garcia, M. Malek Mansour, G. Lie and E. Clementi, *J. Stat. Phys.* **47** 209 (1987).
- [45] D. T. Gillespie, *J. Chem. Phys.* **81** 2340 (1977); D. T. Gillespie, *Markov Processes: An Introduction for Physical Scientists* (Academic Press, New York, 1992).
- [46] C. W. Gardiner, K. J. McNeil, and D. F. Walls, *Phys. Lett. A* **53** 205 (1975).

- [47] F. Baras, M. Malek Mansour and A.L. Garcia, *Phys. Rev. E* **49** 3512 (1994); F. Baras, M. Malek Mansour and A.L. Garcia, *J. Comp. Phys.* **119** 94 (1995).
- [48] J. M. Haile, *Molecular Dynamics Simulation, Elementary Methods*, Wiley, New York (1992).
- [49] P. Resibois and M. De Leener, *Classical Kinetic Theory of Fluids*, (John Wiley and Sons, New York, 1977).
- [50] J. J. Erpenbeck and W. W. Wood, *J. Stat. Phys.* **35** 321 (1984); J. J. Erpenbeck and W. W. Wood, *J. Stat. Phys.* **40** 787 (1985).
- [51] F. Alexander, A. L. Garcia and B. Alder, to appear in *Physica D* (1997).
- [52] D.C. Wadsworth and D.A. Erwin, *AIAA paper* 90-1690 (1990); D.C. Wadsworth and D.A. Erwin, *AIAA paper* 92-2975 (1992); D.B. Hash and H.A. Hassan, *AIAA paper* 95-0410 (1995).
- [53] M. J. Berger and P. Colella, *J. Comp. Phys.* **82** 64 (1989).